Self Calibration and Analysis of the Surphaser 25HSX 3D Scanner

Dr Derek Lichti
Department of Spatial Sciences
Curtin University of Technology
GPO Box U1987
Perth, WA 6845
AUSTRALIA

Stefan Brüstle
Fachschaft Geodäsie
Universität Karlsruhe
Englerstrasse 7
76131 Karlsruhe
GERMANY

Jochen Franke
Scanalyse Pty Ltd
PO Box 1201, Bentley DC 6983
AUSTRALIA

Introduction

- The number of commercially-available AM-CW (phase-shift) TLSs has increased recently
- Examples include
  - Faro LS 840 and LS 880
  - Zoller+Fröhlich IMAGER 5006
  - Leica HDS6000
  - Callidus CPW 8000
  - Surphaser Hemispherical 3D Scanner 25HS/HSX
- We have experience modelling and calibrating the Faro 880
- This presentation reports on an investigation into systematic error modelling and geometric self-calibration of the Surphaser Hemispherical 3D Scanner 25HSX

Surphaser Hemispherical 3D Scanner 25HSX

- Field of view
  - H: full (180°)
  - V: 270°
- Rangefinder performance
  - Short period repeatability with fixed laser spot:
    - 1σ precision @ 10 m: 0.1 mm @ 80% reflectivity, 0.3 mm @ 20%
  - Optimal effective range: 1.5 m to 22 m
- Angular measurement
  - Precision: 15"
  - Maximum resolution: 80 points/°
- Data capture rate: 190 kHz.

Image source http://www.surphaser.com/

Self-Calibration Experiment

- 100 A3-size, circular paper targets were mounted on the walls, floor and ceiling of a room
- Room dimensions: 12.5 m x 7.0 m x 2.6 m
- Eight scans captured from 2 different locations (4 per location), with each differing in κ rotation angle by 90°
- Data captured throughout instrument's full FOV and at least 1.3 m from the nearest wall

Targets

- Faro targets were used since they were readily available
- Faro's contrast centroiding algorithm <u>not</u> used for target measurement, though
- Instead, a specially-designed algorithm was used and will be described later.

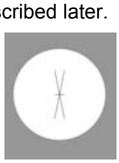

Faro target template

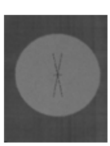

Appearance in Surphaser point cloud

Pre-Processing

- A significant drop-off in return signal intensity existed at longer ranges as we were working with uncorrected data
- Thus, radiometric correction of the intensity was necessary prior to target measurement
- Both linear and histogram equalisation methods were tested but both proved to be inadequate
- A signoid-type function of the following form was therefore used to correct the intensity, e, as a function of range, ρ and dataset-dependent parameters A, b and ρ_0

$$e_i' = A\{2 + \sin[b\pi(\rho - \rho_0)]\}$$

Pre-Processing (cont)

Captured point cloud

Point cloud after radiometric transformation

Target Measurement

- Approximate target centre locations were selected from the 2D projection
- The neighbourhood of target points was then extracted from the 3D point cloud

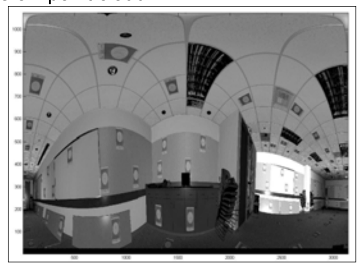

Target Measurement

- Steps in target measurement
  - Best-fit plane of the target points was determined by orthogonal regression
  - 3D data were transformed into the plane co-ordinate system
  - 2D intensity image was resampled from the irregularly-spaced 2D data
  - Edges of the circle were detected
  - The least-squares best-fit circle was computed
  - The inverse transformation of centre co-ordinates was applied and spherical co-ordinates derived

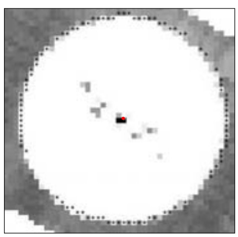

Detected edges and estimated centre

Self-calibration

- Spherical co-ordinate observation equations formed for each target centre (i) in each scan (j)

$$\rho_{ij} + v_{\rho_{ij}} = \sqrt{x_{ij}^2 + y_{ij}^2 + z_{ij}^2} + \Delta\rho$$ Range

$$\theta_{ij} + v_{\theta_{ij}} = \arctan\left(\frac{y_{ij}}{x_{ij}}\right) + \Delta\theta$$ Horizontal direction

$$\alpha_{ij} + v_{\alpha_{ij}} = \arctan\left(\frac{z_{ij}}{\sqrt{x_{ij}^2 + y_{ij}^2}}\right) + \Delta\alpha$$ Elevation angle

where

$$\begin{bmatrix} x_{ij} \\ y_{ij} \\ z_{ij} \end{bmatrix} = R_3(\kappa_j) R_2(\phi_j) R_1(\omega_j) \left\{ \begin{bmatrix} X_i \\ Y_i \\ Z_i \end{bmatrix} - \begin{bmatrix} X_{s_j} \\ Y_{s_j} \\ Z_{s_j} \end{bmatrix} \right\}$$

Rigid body transformation from object space to scanner space

Error Models

- Three additional parameters (APs) were found to be needed (analysis to follow!)

$$\Delta\rho = \varepsilon_{os} + \varepsilon_{int}\alpha_{ij}$$

$$\Delta\theta = 0$$

$$\Delta\alpha = \varepsilon_{ecc}\sin(\alpha_{ij})$$

ε_{os} is the rangefinder offset or zero error
ε_{int} is an elevation-angle dependent range error
ε_{ecc} is the error due to vertical circle eccentricity

Results

- Free-network, self-calibrating adjustment
  - 1515 observations, 1200 df
- RMS of residuals from the adjustments without and with APs

Observable	RMS (without)	RMS (with)
ρ (mm)	±1.1	±1.1
θ (″)	±77.6	±67.2
α (″)	±49.4	±49.2

  - Greatest improvement is in θ, for which, interestingly there are no APs
  - Little or improvement in RMS in other variables, but systematic trends visible, as will be shown shortly

Results (cont)

- Estimated APs and their standard deviations
  - All are small in magnitude but statistically significant

AP	Estimate	σ	| Estimate / σ |
ε_{os} (mm)	-0.7	±0.2	3.82
ε_{int} (mm/° ×10^{-3})	10	±0.95	10.62
ε_{ecc} (″)	58	±11	5.50

Results (cont)

- Evidence of systematic errors in the range residuals as a function of elevation angle and superimposed trend estimate

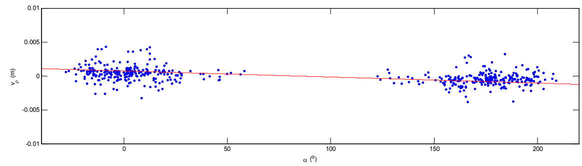

Results (cont)

- Range residuals after self-calibration with error model

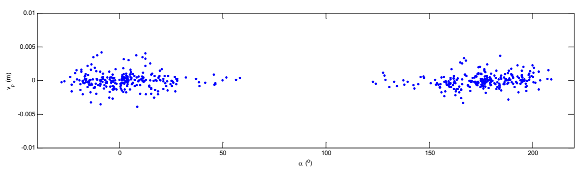

Results (cont)

- Evidence of mass imbalance in the elevation angle residuals as a function of horizontal direction

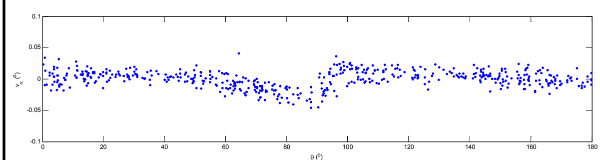

Conclusions

- Results from the calibration show the existence of 3 sources of systematic error:
  - Rangefinder offset
  - Elevation-angle dependent error in range
  - Vertical circle eccentricity
- Though the effects of these errors are small, their estimated additional parameters are statistically significant
- Evidence of mass imbalance in the system was found in the elevation angle residuals when plotted as a function of horizontal direction
- Future work: 3D intensity function fitting for target centre measurement to avoid resampling